Trapping and Frequency Variability in Electron Acoustic Waves

C.F. Driscoll, F. Anderegg, D.H.E. Dubin and T.M. O'Neil

Department of Physics, University of California at San Diego, La Jolla, California 92093 USA

Abstract. Electron Acoustic Waves (EAWs) with a phase velocity less than twice the plasma thermal velocity are observed on pure ion plasma columns. At low excitation amplitudes, the EAW frequencies agree with theory; but at moderate excitation the EAW is more frequency-variable than typical Langmuir waves, and at large excitations resonance is observed over a broad range. Laser Induced Fluorescence measurements of the wave-coherent ion velocity distribution show phase-reversals and wave-particle trapping plateaux at $\pm v_{ph}$, as expected, and corroborate the unusual role of kinetic pressure in the EAW.

Keywords: add some here
PACS: 52.27.Jt, 52.35.Fp, 52.35.Sb

Electron Acoustic Waves (EAWs) are the low frequency branch of electrostatic plasma (Langmuir) waves. The EAW typically has a phase velocity $v_{ph} \sim 1.4\bar{v}$ (for small $k\lambda_D$), quite low compared to typical plasma waves, and its frequency has a strong temperature dependence, $f_{EAW} \propto T^{1/2}$. Linear Landau damping would suggest that such slow phase velocity waves are strongly damped; but at finite wave amplitudes, trapping of particles near the phase velocity "flattens" the distribution function, resulting in a weakly damped wave.

These waves have been studied theoretically [1, 2] and numerically [3]; they have been observed in experiments with pure electron plasmas [4] and in laser-produced plasmas [5, 6] and related numerical simulations [7, 8]. The same name is applied to substantially different waves on bi-Maxwellian distributions in space physics [9]; but here we focus on near-Maxwellian plasmas only. Here, we observe EAWs in pure ion plasmas, where the ions are the mobile species and "EAW" is somewhat of a misnomer. However, the characteristics of EAWs are the same for mobile ions as for mobile electrons.

In experiments, we observe that at small amplitude, the EAW dispersion relation is correctly described by the "principal-part" approach of Holloway and Dorning [1]. In contrast at larger amplitude we observe that we can excite an EAW wave at "any" frequency in the range of $1.4\bar{v} < v_{ph} < 2.1\bar{v}$; under these conditions, there is no simple dispersion relation for these waves. That is, the excitation modifies the particle distribution so as to make the wave resonant with the excitation frequency. This is similar to results from Vlasov-Poisson simulations [10] in the highly non-linear amplitude regime, suggesting that EAW-like modes with strong harmonic content, called KEEN waves, can be excited over a wide range of frequencies.

EXPERIMENTAL APPARATUS

We observe slow (EAW) and fast (Langmuir or Trivelpiece-Gould) waves in pure ion plasmas, both being azimuthally-symmetric standing waves. We use a Mg^+ ion plasma confined in a Penning-Malmberg trap [11] with a uniform magnetic field $B = 3$ Tesla. Figure 1 shows the trap consisting of a series of hollow conducting cylinders of radius $R_w = 2.86$ cm contained in ultrahigh vacuum at $P \approx 10^{-10}$ Torr. The ion density is $n \sim 1.5 \times 10^7$ cm^{-3}, over a radius $R_p \approx 0.45$ cm, with length $L_p \simeq 9$ cm. The plasma ions are held in *steady state* for days, by utilizing a weak "rotating wall" electric field [12] applied to the sectored electrode. The rotating wall is turned off about 100 ms before each wave measurement and is restored about 200 ms later, and the plasma re-equilibrates to a Maxwellian distribution during a 5-sec period between wave excitations.

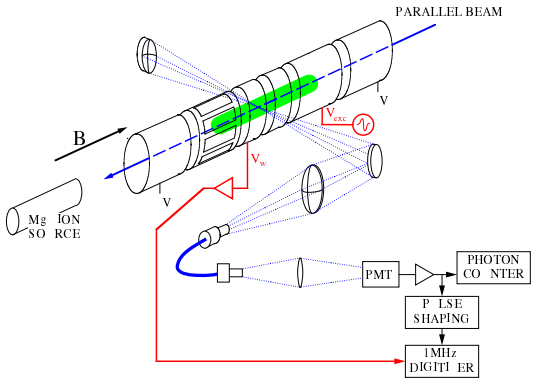

FIGURE 1. Experimental setup with coherent photon detection.

A diagnostic laser beam parallel to the magnetic field close to the trap axis illuminates the plasma, and Laser Induced Fluorescent (LIF) photons are collected by optics perpendicular to the trap axis. The diagnosed volume is the intersection of the laser beam with the viewing volume of the detection optics, corresponding to about a volume of length $\Delta z_L = 0.3$ cm and of radius $\Delta r_L \simeq 0.1$ cm. Individual detected photons emitted in the diagnosed volume are counted and their time of arrival recorded. The laser beam comes from a frequency-doubled dye laser and is tuned across the cyclic ${}^2S_{1/2}^{m_j=-1/2} \rightarrow {}^2P_{3/2}^{m_j=-3/2}$ (280 nm) transition from the ground state of singly ionized magnesium ions.

For the data presented here, the pre-wave plasma has a LIF-measured Maxwellian velocity distribution, with temperature controlled in the range 0.3 eV $< T < 1.5$ eV. These plasma parameters give Debye length 0.1 cm $< \lambda_D < 0.24$ cm, thermal velocities 110 cm/ms $< \bar{v} < 245$ cm/ms, ion-ion collision rate 8 sec$^{-1} > \nu_{ii} > 0.7$ sec^{-1}, and plasma frequency $f_p = 165$ kHz.

We excite standing EAW and TG waves with an electrode located near the end of the plasma column, and detect the waves with a separate cylinder located near the other end of the plasma. Both excitation and detection electrodes are azimuthally symmetric and so only excite and detect azimuthally symmetric modes ($m_\theta = 0$). The modes presented

in this paper have the longest possible axial wavelength ($m_z = 1$), that is $\lambda \approx 2L_p$, and the lowest radial mode number ($m_r = 1$). The EAWs are excited by an amplitude-rounded burst $V_{\rm exc}(t)$ of N_c cycles at a frequency $f_{\rm exc}$ and amplitude $A_{\rm exc}$ applied to the wall cylinder. Without amplitude rounding the TG wave is also excited by the harmonic content of the burst.

The wave-induced wall voltage $V_w(t)$ is then recorded, and is fit in overlapping time segment as

$$V_w(t) = A_w(t)\cos(\theta_w(t)) \tag{1}$$

resulting in $\theta_w(t)$ with slowly varying $A_w(t)$ and frequency $f_w(t) = d\theta_w/2\pi dt$. This wave phase will be used for wave-coherent measurements of the ion motion.

Figures 2a, b show typical resonant excitation and reception waveforms for the TG and EAW waves. The TG wave is readily excited by $N_c = 10$ cycles at amplitude $A_{\rm exc} =$ 2 mV. In contrast, the EAW is excited to similar amplitude by $N_c = 100$ with $A_{\rm exc} =$ 200 mV. Moreover, the TG wave grows smoothy with excitation, whereas the EAW wave shows an erratic response for hundreds of cycles of excitation. These received waveforms show $\gamma_{\rm TG} \sim 10/\text{sec}$, and $\gamma_{\rm EAW} \sim 100/\text{sec}$. However, if the EAW excitation had been terminated after 20 cycles, the resulting wave would show $\gamma_{\rm EAW} > 10^3/\text{sec}$.

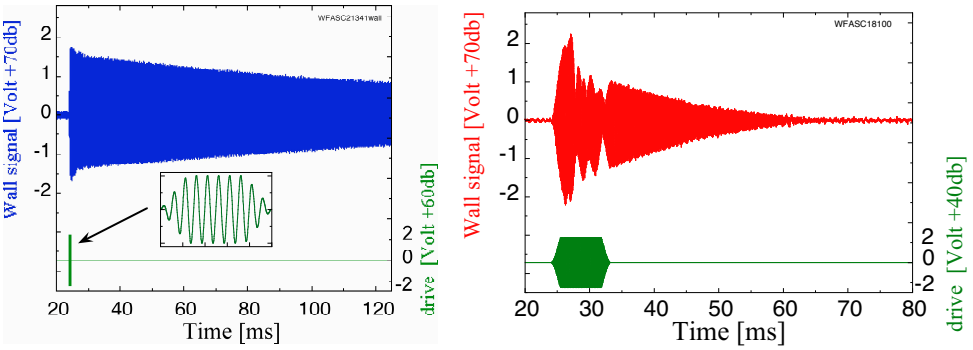

FIGURE 2. a) Detected EAW wall signal $V_w(t)$ and drive burst $V_{\rm exc}(t)$ at $f_{\rm exc} = 21.5$ kHz. b) Detected EAW wall signal $V_w(t)$ and 100 cycles drive burst $V_{\rm exc}(t)$ at $f_{\rm exc} = 10.7$ kHz.

DISPERSION RELATION

In an infinite homogeneous unmagnetized plasma, the dispersion relation for an electron acoustic wave of wavenumber $\mathbf{k} = k\hat{z}$ and frequency ω is

$$\omega_p^2 \oint d\mathrm{v}_z \frac{\partial F_0/\partial \mathrm{v}_z}{\mathrm{v}_z - \omega/k} = k^2 \tag{2}$$

where $\omega_p = \sqrt{4\pi e^2 n/m}$ is the plasma frequency. Here, $F_0(\mathrm{v}_z) = \int d\mathrm{v}_x d\mathrm{v}_y F_0(\mathbf{v})$ is the equilibrium velocity distribution for velocity component v_z, and the integral is the "principal part" of the Landau contour integral [1]. The principal part is used instead of the Landau contour because it is presumed that the waves have modified F_0, "flattening" the distribution over a small (i.e. negligible) range of velocities around the phase speed

ω/k. Assuming that F_0 is a Maxwellian distribution at temperature T, Eq. (2) may be solved for ω and the resulting "thumb diagram" is shown in Fig. 3a. The upper branch is the traditional Langmuir wave, asymptoting to ω_p for $k_z\lambda_D = 0$. The lower branch (EAW) has an acoustic dispersion relation for small $k_z\lambda_D$.

In a plasma column of radius R_p confined in a trap of radius R_w, the dispersion relation is modified and the Langmuir wave becomes acoustic also, as first analyzed by Trivelpiece and Gould [13], here TG. Moreover, for finite plasma length L_p, the waves are bi-directional and standing, with specific axial wavenumbers given approximately by $k_z = m_z\pi/L_p$, $m_z = 0, 1, 2, ...$ The modes have an electrostatic potential structure of the form

$$\delta\phi(r,\theta,z) = \cos(k_z z)e^{im_\theta\theta}\Phi_{mk_z}(r) \tag{3}$$

where $\Phi_{m_\theta k_z}$ satisfies

$$\left[\frac{1}{r}\frac{\partial}{\partial r}r\frac{\partial}{\partial r} - \frac{m_\theta^2}{r^2} + \omega_p^2(r)\int\!\!\!\!\!\!-\frac{d\mathrm{v}_z\,\partial F_0/\partial \mathrm{v}_z}{\mathrm{v}_z - \omega/k_z}\right]\Phi_{m_\theta k_z}(r) = 0 \tag{4}$$

with boundary conditions that $\Phi \propto r^{m_\theta}$ near $r = 0$ and $\Phi_{m_\theta k_z} = 0$ at $r = R_w$. Here $\omega_p(r) = \sqrt{4\pi e^2 n(r)/m}$ is the plasma frequency for density $n(r)$.

Equation (4) is an eigenvalue problem for the frequency ω, and can be solved numerically for given F_0, m_θ and k_z via the shooting method. For the case of a top-hat density profile with $n(r) = n_0$ for $r < R_p$ and zero otherwise, a solution to Eq. (4) for $\Phi_{m_\theta k_z}(r)$ can be obtained in terms of Bessel functions [14].

In Fig. 3b $\omega(k_z)$ is plotted for the case where $k_\perp\lambda_D = 0.25$, from $(\lambda_D/R_p)\ [2/\ln(R_w/R_p)]^{1/2} = 0.25$. In Fig. 3c this dispersion relation is plotted versus temperature at fixed $k_z = \pi/L_p$. Also, to compare the experiments it is important to use the actual radial density profile $n(r)$ rather than a top-hat profile, so in obtaining the dashed line of Fig. 3c the numerical shooting solution was employed.

When the amplitude is turned down sufficiently ($A_{\mathrm{exc}} \lesssim 50$ mV), the standing waves are observed at only specific isolated frequencies, plotted in Fig. 3c as dots (EAW) and squares (TG wave). At small amplitude, these measurements are well described by the near linear theory of Refs. [1] and [3], including the expected temperature dependence for these moderately high temperatures. At temperatures above 1.3 eV, no waves are observed at comparably low excitation amplitude.

However, with larger amplitude excitation, the waves are excited over a range of frequencies; and furthermore, they ring at frequencies different than f_{EAW} or f_{exc} because the excitation has significantly modified the distribution function. The gray bar at $T = 0.8$ eV shows the range of frequencies over which a 100 cycle burst with $A_{\mathrm{exc}} = 300$ mV resulted in a wave $f_w = f_{\mathrm{exc}}$ ringing for hundreds of cycles. This means that at $T = 0.8$ eV, a wave can be excited at "any frequencies" within the vertical extent of the gray bar. We emphasize that the axial wavenumber k_z does not change; rather, the phase velocity of the wave is changing. Similarly, plasma waves at $T = 1.4$ eV are excited with $A_{\mathrm{exc}} = 200$ mV for 100 cycles, past the "end of the thumb" as shown by the gray bar where no near-linear solution exists. The drive modifies the particle distribution until the distribution becomes resonant with the drive. Naming waves in these continuous regime is ill defined, since wave names are generally given for well characterized

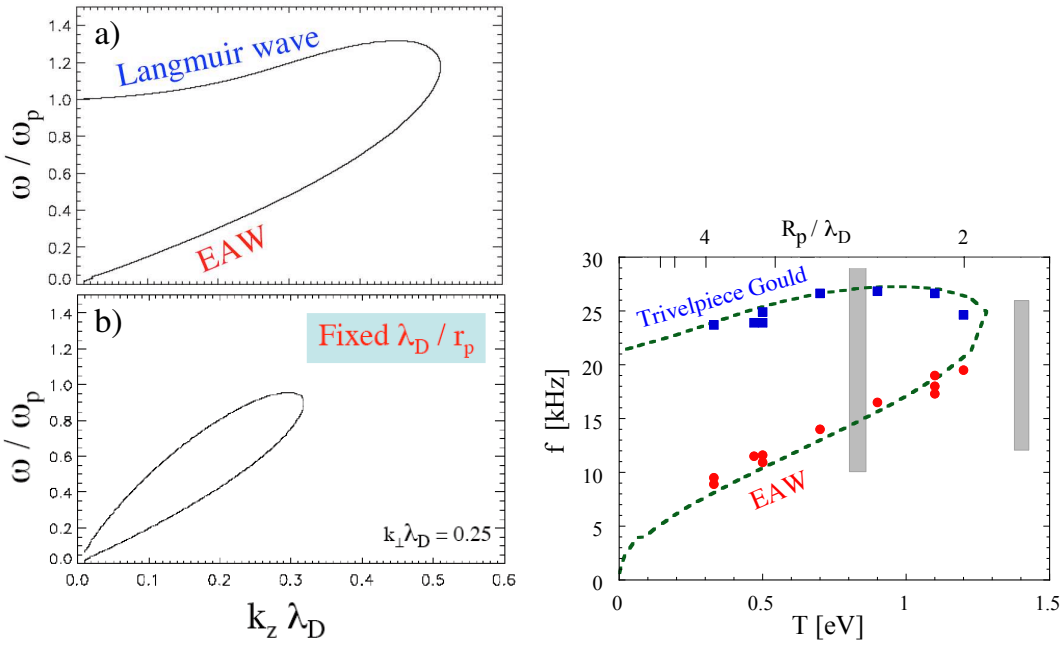

FIGURE 3. Plasma wave dispersion relation in (a) homogeneous, infinite plasma; (b) plasma of finite radial size; (c) Plasma wave dispersion relation for finite radial size plasma and fixed k_z, plotted versus temperature.

distributions such as Maxwellian or near-Maxwellian distribution functions and beams. It is worth noting that Skiff *et al.* [15] observed a new branch of electrostatic wave on slightly non-Maxwellian plasmas.

COHERENT PARTICLE DISTRIBUTION MEASUREMENT

The LIF data allow us to construct the particle distribution function $F(\mathrm{v},\theta)$ coherent with the wave phase $\theta_w(t)$ received on the wall. The excitation laser propagates axially at $r=0$, with frequency tuned to be resonant with particles of velocity v_ℓ. The individual fluorescent photons emitted from the central axial region of the plasma are detected. The rate of detected photons is $P(\mathrm{v}_\ell,t)$ representing $F(\mathrm{v}_\ell,z=0,t)$. We calculate the correlation integral

$$\delta F^{\mathrm{coh}}(\mathrm{v}_\ell)=\int_{t_1}^{t_2} dt\left(\frac{P(\mathrm{v}_\ell,t)}{t_2-t_1}\right)\cos[\theta_w(t)-\theta_{w0}] \tag{5}$$

for a period t_2-t_1 encompassing about 1000 photons over about 100 wave cycles. Repeating this process for 250 velocities v_ℓ results in $\delta F^{\mathrm{coh}}(\mathrm{v}_\ell)$. Each measurement is on the same plasma, after waiting ~ 5 sec for the plasma to re-equilibrate.

Figure 4(a) shows the wave-phase coherent $\delta F^{\mathrm{coh}}(\mathrm{v})$ in the presence of a moderate amplitude standing EAW at 10.7 kHz. The change of sign at $\mathrm{v}=0$ comes from the

$\partial F/\partial \mathrm{v}$ term, and the sign change at $\pm \mathrm{v_{ph}}$ comes from the $(\mathrm{v}-\mathrm{v_{ph}})$ term in the denominator of Eq. (2). The zero crossings at $\pm \mathrm{v_{ph}}$ are an experimental measurement of the standing wave phase velocity. Here $\mathrm{v_{ph}} = \pm 208$ cm/ms gives $\frac{1}{2}\lambda = \mathrm{v_{ph}}/2f = 9.7$ cm; this is about 10% longer than L_p, as is typical of standing plasma waves in traps [16]. The solid line is the result of a simple model representing the superposition of two *independent* waves traveling with $\pm \mathrm{v_{ph}}$ on separate Maxwellian distributions [14].

Figure 4(b) shows the particle distribution $F_0(\mathrm{v})$ before the wave, with a temperature $T = 0.31$ eV. As the wave damps, the wave energy is transferred to the particles resulting in a temperature increase to $T = 0.44$ eV measured 100 ms later.

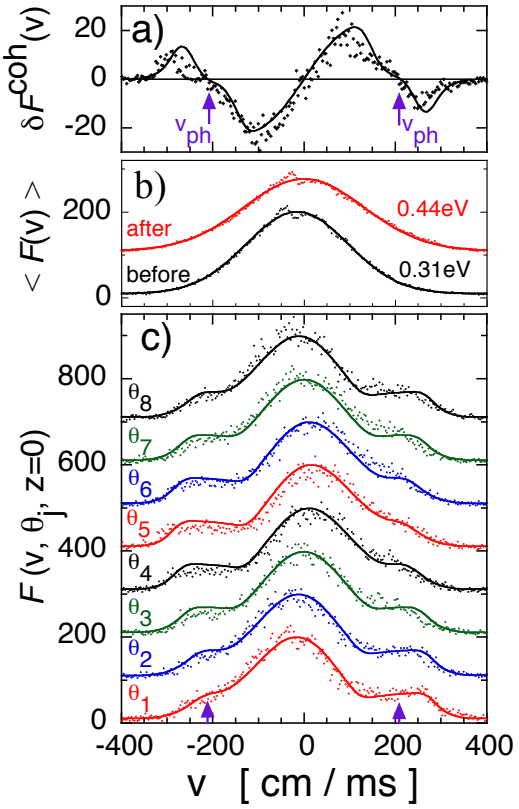

FIGURE 4. (a) Coherent particle response $\delta F(\mathrm{v})$. (b) Phase average particle distribution before and after EAW. (c) Phase-coherent particle distribution in the presence of an EAW with $\mathrm{v_{ph}} = 208$ cm/ms.

A similar wave-coherent LIF technique gives the particle distribution $F(\mathrm{v},\theta_j)$ at various wave phases, by binning the received photons into 8 wave-phase bins $\theta_j = 2\pi j/8$, shown in Fig. 4(c). To obtain these we accumulate photons in their respective phase bins for 10 ms, that is ~ 100 wave cycles. $F(\mathrm{v},\theta_j)$ show two plateaux, corresponding to the particles trapped by the wave at $\pm \mathrm{v_{ph}}$. The widest plateaux $\Delta \mathrm{v}_T$ are observed at phase $\theta_j = 1$ and 5. These wave-trapped particles propagate in the wave troughs past the photon detector at $z = 0$, and reflect at the plasma ends, remaining trapped during hundreds of end reflections. Figure 4(c) also shows clearly the oscillations back and forth ($\delta \mathrm{v}_0$) of low velocity (non-trapped) particles. The solid curves on Fig. 4(c) are the result of the standing wave model.

This same data is better visualized in the contour plot of Fig. 5, where the 8 phase-bins are interpolated to make the wave-phase x-axis. The color (grey) scale represents the measured $F(\mathrm{v},\theta)$, and the curves represent the simple 2-wave theory model. The plateaux of Fig. 4 are the "cat's eye" trapping regions of Fig. 5, with maximal velocity width $2\Delta V_T$; and the $\delta \mathrm{v}_0$ oscillation of the bulk Maxwellian is seen near $\mathrm{v}=0$.

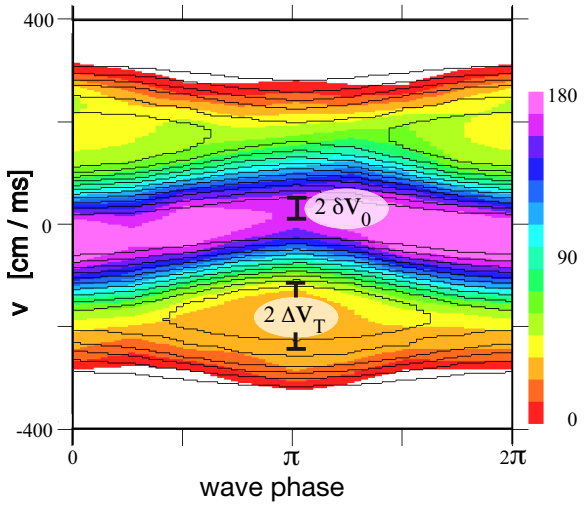

FIGURE 5. Contour plot of $F(\mathrm{v},\theta_j)$ measured at $z=0$.

Note that Fig. 5 is $F(\mathrm{v},\theta;z=0)$ rather than the usual theory phase-space plot of $F(\mathrm{v},z;t)$. In phase-space, the upper trapping regions would move right with time t, reflecting into the lower left-moving trapping regions at the right-hand edge. A similar effect would be seen experimentally if the position of the LIF could be scanned in z.

We also note that the persistence of these BGK trapping states is somewhat surprising, in that it requires that the wave and the particles reflect at the same z-positions on the ends. In actuality, the wavelength is somewhat larger than $2L_p$, and the reflection point for a particle depends on its kinetic energy. One might expect that some "untrapping" would occur at the ends, resulting in damping of the wave. However, this effect has not yet been observed or analyzed.

From a fluid perspective, the low frequency and frequency variability of the EAW can both be understood as resulting from the unusual negative dynamical compressibility. A positive density perturbation δn consists of an increase in particles with $\mathrm{v} \lesssim \mathrm{v}_{\mathrm{ph}}$, and a decrease in particles with $\mathrm{v} \gtrsim \mathrm{v}_{\mathrm{ph}}$, as shown in Fig. 4a. The positive δn gives a positive restoring potential $\delta\phi$ (as for a Langmuir wave); but it gives a *negative* restoring pressure $\delta\mathscr{P}$, due to the v^2 weighting. In the EAW, the restoring $\delta\phi$ is almost totally cancelled by $\delta\mathscr{P}$, giving a low frequency. Moreover, this cancellation is quite sensitive to $f(\mathrm{v})$ near v_{ph}, so small changes in $f(\mathrm{v})$ result in large frequency changes. In contrast, the pressure term is small for Langmuir waves at low temperatures, and the frequency is relatively independent of $f(\mathrm{v})$.

DISCUSSION

We have observed near-linear plasma waves with a phase velocity slow enough to be located in the bulk of the particle velocity distribution, generically called Electron Acoustic Waves. At small amplitude, the experimentally observed standing wave frequencies confirm the theory concept of Holloway and Dorning presuming a local "flattening" of the particle distribution around the phase velocity. At moderate and large amplitude, the waves can be excited over a wide continuum range of frequencies. Here the wave driver modifies the particle velocity distribution until the distribution becomes resonant with the drive. The observed mode frequency is still surprisingly well described by the Dorning theoretical approach using the modified particle distribution, even for the large amplitude case.

ACKNOWLEDGMENTS

We thank Dr. B. Afeyan and Dr. R.W. Gould for stimulating discussions. This work was supported by National Science Foundation grants PHY-0354979 and PHY-0903877 and NSF/DOE grant PHY-0613740.

REFERENCES

1. J.P. Holloway and J.J. Dorning, Phys. Rev. A **44**, 3856 (1991).
2. H. Schamel, Phys. Plasmas **7**, 4831 (2000).
3. F. Valentini, T.M. O'Neil and D.H.E. Dubin, Phys. Plas. **13**, 052303 (2006).
4. A.A. Kabantsev, F. Valentini, and C.F. Driscoll, in NNP VI (edited by M. Drewsen *et al.*, eds.), AIP Conf. Proc. **862**, 13 (2006); F. Valentini, T.M. O'Neil and D.H.E. Dubin, AIP Conf. Proc. **862**, 3 (2006).
5. D.S. Montgomery, R.J. Focia, H.A. Rose, D.A. Russell, J.A. Cobble, J.C. Fernández, and R.P. Johnson, Phys. Rev. Lett. **87**, 155001 (2001).
6. N.J. Sircombe, T.D. Arber and R.O. Dendy, Plas. Phys. and Control. Fusion **48**, 1141 (2006).
7. Lj. Nikolić, M.M. Ŝkorić, S. Ishiguro, and T. Sato, Phys. Rev. E **66**, 036404 (2002).
8. A. Ghizzo, T.W. Johnston, T. Révéille, P. Bertrand, and M. Albrecht-Marc, Phys. Rev. E **74**, 046407 (2006); T.W. Johnston, Y. Tyshetskiy, A. Ghizzo and P. Bertrand, Phys. Plasmas **16**, 042105 (2009).
9. I. Kourakis and P.K. Shukla, Phys. Rev. E **69**, 036411 (2004).
10. B. Afeyan, K. Won, V. Savchenko, T.W. Johnston, A. Ghizzon, and P. Bertrand, Proc. Inertial Fusion Sciences and Applications 2003 (B. Hamel, *et al.*, eds.), Monterey: American Nuclear Society (2004), p. 213.
11. F. Anderegg, X.-P. Huang, E. Sarid, and C.F. Driscoll, Rev. Sci. Instrum. **68**, 2367 (1997).
12. X.-P. Huang, F. Anderegg, E.M. Hollmann, C.F. Driscoll and T.M. O'Neil, Phys. Rev. Lett. **78**, 875 (1997); F. Anderegg, E.M. Hollmann, and C.F. Driscoll, Phys. Rev. Lett **81**, 4875 (1998); E.M. Hollmann, F. Anderegg, and C.F. Driscoll, Phys. Plasmas **7**, 2776 (2000).
13. A.W. Trivelpiece and R.W. Gould, J. Appl. Phys. **30**, 1784 (1959).
14. F. Anderegg, C.F. Driscoll, D.H.E. Dubin, T.M. O'Neil and F. Valentini, Phys. Plasmas **16**, 055705 (2009); F. Anderegg, C.F. Driscoll, D.H.E. Dubin and T.M. O'Neil, Phys. Rev. Lett. **102**, 095001 (2009).
15. F. Skiff, H. Gunell, A. Bhattcharjee, C.S. Ng, and W.A. Noonan, Phys. Plasmas **9**, 1931 (2002).
16. J.K. Jennings, R.L. Spencer and K.C. Hansen, Phys. Plasmas **2**, 2630 (1995).